J Paleolimnol (2013) 50:275–291
DOI 10.1007/s10933-013-9723-9

ORIGINAL PAPER

# Origin and significance of diagenetic concretions in sediments of Laguna Potrok Aike, southern Argentina

**A. Vuillemin · D. Ariztegui · A. S. De Coninck · A. Lücke · C. Mayr · C. J. Schubert · The PASADO Scientific Team**

Received: 7 June 2012 / Accepted: 30 April 2013 / Published online: 14 May 2013


**Abstract** Authigenic minerals can form in the water column and sediments of lakes, either abiotically or mediated by biological activity. Such minerals have been used as paleosalinity and paleoproductivity indicators and reflect trophic state and early diagenetic conditions. They are also considered potential indicators of past and perhaps ongoing microbial activity within sediments. Authigenic concretions, including vivianite, were described in late glacial sediments of Laguna Potrok Aike, a maar lake in southernmost Argentina. Occurrence of iron phosphate implies specific phosphorus sorption behavior and a reducing environment, with methane present. Because organic matter content in these sediments was generally low during glacial times, there must have been alternative sources of phosphorus and biogenic methane. Identifying these sources can help define past trophic state of the lake and diagenetic processes in the sediments. We used scanning electron microscopy, phosphorus speciation in bulk sediment, pore water analyses, in situ ATP measurements, microbial cell counts, and measurements of methane content and its carbon isotope composition ($\delta^{13}C_{CH4}$) to identify components of and processes in the sediment. The multiple approaches indicated that volcanic materials in the catchment are important suppliers of iron, sulfur and phosphorus. These elements influence primary productivity and play a role in microbial metabolism during early diagenesis. Authigenic processes led to the formation of pyrite framboids and revealed sulfate reduction. Anaerobic oxidation of methane and shifts in pore

**Electronic supplementary material** The online version of this article (doi:10.1007/s10933-013-9723-9) contains supplementary material, which is available to authorized users.

A. Vuillemin (✉) · D. Ariztegui
Section of Earth and Environmental Sciences, University of Geneva, rue des Maraîchers 13, 1205 Geneva, Switzerland
e-mail: aurele.vuillemin@unige.ch

A. S. De Coninck
Water Earth Environment Center, National Institute of Scientific Research, rue de la Couronne 490, Quebec, QC G1K 9A9, Canada

A. Lücke
Institute of Bio- and Geosciences IBG- 3: Agrosphere, Research Center Jülich, 52425 Jülich, Germany

C. Mayr
Institute of Geography, University of Erlangen-Nürnberg, Kochstr. 4/4, 91054 Erlangen, Germany

C. Mayr
Geobio-Center and Department of Earth and Environmental Sciences, University of Munich, Richard-Wagner-Str. 10, 80333 Munich, Germany

C. J. Schubert
Department of Surface Waters-Research and Management, Eawag, Swiss Federal Institute of Aquatic Science and Technology, Seestr. 79, 6047 Kastanienbaum, Switzerland

water ion concentration indicated microbial influence with depth. This study documents the presence of active microbes within the sediments and their relationship to changing environmental conditions. It also illustrates the substantial role played by microbes in the formation of Laguna Potrok Aike concretions. Thus, authigenic minerals can be used as biosignatures in these late Pleistocene maar sediments.

**Keywords** Authigenic minerals · Microbial reduction · Methanogenesis · Vivianite · Framboids · ICDP-project PASADO

## Introduction

Formation of authigenic minerals in lacustrine systems has been reported in the water column (Böttcher and Lepland 2000), at the sediment–water interface (Manning et al. 1999), and within sediments (Berner 1981). Such mineral formation can occur as a consequence of saturated ion concentrations (Wilkin and Arthur 2001), and/or early diagenetic processes such as organic matter (OM) decomposition (Berner 1981) and microbial activity (Beveridge et al. 1983). Thus, these minerals poorly reflect their initial sedimentary settings. Indeed, the evolution of reducing conditions in the sediment (Berner 1981) and pore waters (Emerson 1976) is known to control the formation, transformation and preservation of authigenic minerals, as they go through complex stages involving precipitation, amorphous phases (Glasauer et al. 2003) and precursors (Wilkin and Barnes 1997).

In lakes, the formation of iron minerals can be either syngenetic or diagenetic (Wilkin and Barnes 1997; Fagel et al. 2005). Hydrous ferric oxide (HFO) derived from goethite (FeO(OH)) and limonite ($FeO(OH)\cdot nH_2O$) can be further transformed into diagenetic forms of reduced iron such as magnetite ($Fe_3O_4$), siderite ($FeCO_3$) and vivianite ($Fe_3^{2+}(PO_4)_2\cdot 8H_2O$) (Zachara et al. 1998; Konhauser 2007). In freshwater basins, precipitation and dissolution of iron phosphates are important mechanisms that regulate phosphorus concentration in the water column (Nriagu and Dell 1974). Formation of iron phosphates results from phosphorus adsorption and sinking to the sediments (Gächter et al. 1988; Wang et al. 2007), processes that primarily depend on water-column conditions such as salinity, density stratification of the water body, presence of iron oxides (Wilson et al. 2010) and the nature of sedimented clay minerals (Stamatakis and Koukouzas 2001). Phosphorus sorption on HFO often results in the formation of "green rust" which is a main amorphous precursor of iron phosphate minerals (Fredrickson et al. 1998). Nonetheless, reduction of Fe(III) is required to form most of those minerals. In the sediment, where microbes show stronger catalyzing capacity than in the water column (Lovley 1997), dissolved ions (Nriagu 1972), OM mineralization (Emerson 1976) and reactivity linked to nutrient recycling (Anderson et al. 2001) are additional factors that are influenced by microbes and affect authigenic minerals. Especially under eutrophic conditions (Hupfer et al. 1998; Manning et al. 1999), microbial communities (Nealson and Stahl 1997) have been invoked as contributors to early and shallow-burial formation of authigenic minerals. OM decay and microbial activity produce humic and gel-like substances that promote supersaturated conditions in pore waters (Zelibor et al. 1988), resulting in the crystallization of aggregates. Different degrees of hypoxia and various pore water chemistries (e.g. iron, phosphate, sulfide) can be generated by microbial processes, thus leading to specific mineral phases and specific crystal shapes (Postma 1981; Glasauer et al. 2003; Konhauser 2007). For example, in the presence of dissolved Fe(II), methanogenesis and sulfate reduction promote mainly vivianite and pyrite formation. Under reducing conditions, vivianite is the most stable iron phosphate (Emerson 1976; Berner 1981), thus exerting significant control over Fe and P geochemical cycles (Nriagu 1972). Yet production of $H_2S$ via sulfate reduction tends to destabilize and scavenge iron from its structure (Nriagu 1972). Coexistence of pyrite and vivianite in Laguna Potrok Aike concretions requires investigation, as microbial communities commonly develop competitive or synergetic behaviors (Nauhaus et al. 2002). Furthermore, dissimilatory iron-reducing bacteria (DIRB), sulfate-reducing bacteria (SRB) and even methanogens (Zhang et al. 2012) not only oxidize OM while reducing iron (Fredrickson et al. 1998; Zachara et al. 1998), but sometimes alter minerals (Stucki and Kostka 2006) and associated sediment properties (Kostka et al. 1999; Dong et al. 2009).

Previous geomicrobiological studies of Laguna Potrok Aike sediments, southern Argentina, demonstrated the influence of endogenic, layered microbial

communities (Nealson and Stahl 1997) on surficial sediments and their ability to recycle nutrients (Vuillemin et al. 2012). The discovery of vivianite concretions in deep, glacial-age sediments (Nuttin et al. 2012) offers the opportunity to infer prevailing bottom-water conditions and inputs to sediments at the time of vivianite formation. It also presents an opportunity to elucidate the possible role of microbes in the development of the concretions, during both early diagenesis and following deep burial. Lastly, it provides a chance to better define the depths of formation for such minerals and the microbial processes involved in authigenesis. Use of the concretions as paleoindicators or microbial biosignatures can help address aspects of the phosphorus cycle, both in the water column and via microbial activity within the sediments.

This study combines geochemistry, such as chemical separation of different phosphorus forms (i.e. P speciation), total organic carbon (TOC), methane content, carbon isotopes ($\delta^{13}C_{org}$, $\delta^{13}C_{CH4}$) and pore water analyses, with microbiological evidence for microbial life, such as in situ ATP (adenosine-triphosphate) detection and DAPI (4′, 6-diamidino-2-phenylindole) cell counts. Additionally, scanning electron microscopy (SEM) allowed high magnification imagery of the different mineral phases that were identified using X-ray energy spectroscopy (EDS).

### Site description

Laguna Potrok Aike (52°S/70°W) is a maar lake in the Pali Aike volcanic field of southern Patagonia, Argentina (Zolitschka et al. 2006). Catchment lithology is dominated mainly by mafic volcanics (Fig. 1), whereas carbonates are absent. Today, the lake has a maximum diameter of 3.5 km, an area of 7.74 $km^2$ and a maximum water depth of 100 m. Annual precipitation ranges between 200 and 300 mm, reflecting the semi-arid climate of the area. Average wind speed is 7.4 m/s and annual temperature extremes range between 33 °C and −16 °C. Potrok Aike is one of the few permanent water-filled lakes in the southeastern Patagonian steppe, making its sediment record important for paleoclimate reconstructions (Haberzettl et al. 2007). Its seismic stratigraphy has been extensively studied (Anselmetti et al. 2009; Gebhardt et al. 2011), as have its sediment OM sources (Mayr et al. 2009). Today the lake is polymictic, with a non-stratified water column and oxygenated bottom waters. It displays low productivity because of subsaline conditions and is considered mesotrophic (Zolitschka et al. 2006). Haberzettl et al. (2007) examined bulk element ratios in sediments and suggested that oxic to suboxic conditions have prevailed at the water/sediment interface. Other sediment features, however, such as color and grain size, along with the presence of biogenic methane in very shallow sediments (Vuillemin et al. 2012), point to limited oxygen penetration below the water/sediment interface. Recently, the study of five sediment cores retrieved through the ICDP-sponsored PASADO project enabled inference of past lake-level fluctuations (Kliem et al. 2012; Ohlendorf et al. 2012) and paleoclimate reconstruction for the late Pleistocene and Holocene (Recasens et al. 2012).

## Materials and methods

### Sampling strategy

For this study, we utilized two hydraulic piston cores retrieved from the center of the lake, at 100 m water depth (Fig. 1). Cores 5022-1A and 5022-1D were 65 mm in diameter, with respective lengths of 87 and 97 m, with a sediment record encompassing at least 55 ka (Kliem et al. 2012). Core 5022-1D was sampled in the field for geomicrobiological studies. A special subsampling protocol was applied to minimize contamination risks and is described in detail elsewhere (Vuillemin et al. 2012). Sampling windows were cut in the core liners to facilitate quick sampling under semi-aseptic conditions in the field laboratory. Specific conditioning was applied to sediments for methane headspace analyses, DAPI cell counts, and in situ ATP detection assessment (Vuillemin et al. 2012). Core 5022-1A was sealed and stored at 4 °C, and sampled for pore water analyses in Bremen, Germany. Core 5022-1D was resampled for standard bulk analyses. Vivianite concretions (Nuttin et al.2012) were sampled in three cores from site 2 (Fig. 1). Corresponding depths in cores from site 1 were obtained by correlation using magnetic susceptibility profiles (Recasens et al. 2012). Correlation was confirmed by the presence of similar authigenic minerals at corresponding depths in the core from site 1, documented using digital pictures of opened core 5022-1D (Fig. 2). A

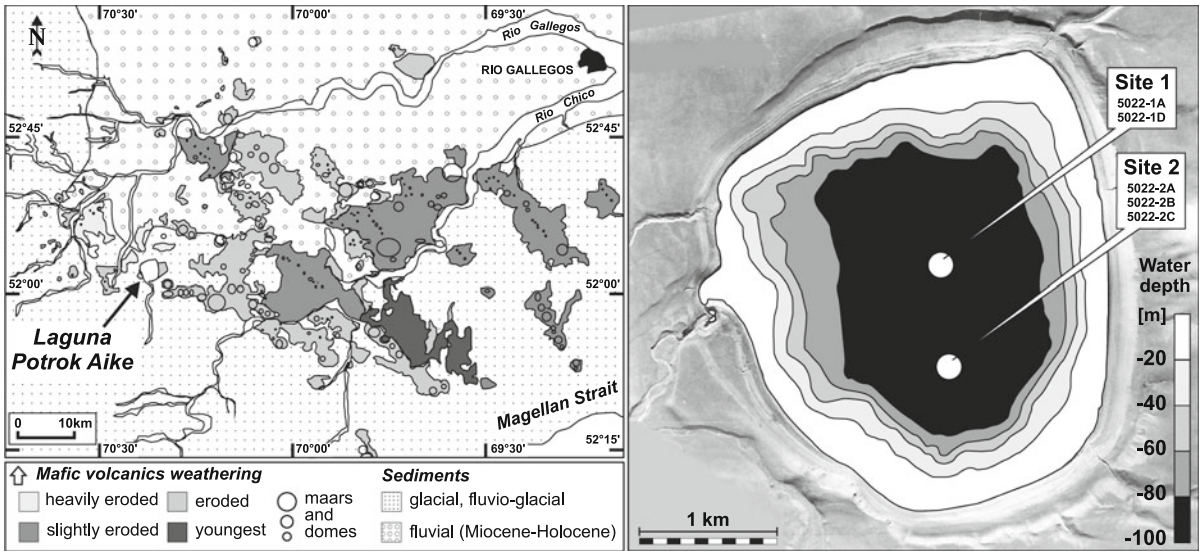


**Fig. 1** *Left* Map of the Pali Aike volcanic field (modified after Ross et al. 2011) displaying the location of Laguna Potrok Aike within its catchment. The catchment area represents some 200 km$^2$ (Ohlendorf et al. 2012). *Right* Bathymetric map of Laguna Potrok Aike (modified after Zolitschka et al. 2006) showing the two drilling sites and the cores sampled in the present study

complete stratigraphic record of the 5022-1D core and sample depths is available in electronic supplementary material (ESM 1).

## Analyses

Methods for determination of methane headspace, phosphorus speciation, in situ ATP detection and DAPI cell counts were published (Vuillemin et al. 2012).

Total organic carbon (TOC), total nitrogen (TN) and the stable carbon isotope composition ($\delta^{13}C_{org}$) of the homogenized bulk organic fraction were analyzed on decalcified and untreated samples, respectively, using an elemental analyzer (EuroVector®, Euro EA®) linked by continuous flow to an isotope-ratio mass spectrometer (Micromass, IsoPrime®). Isotope ratios are reported in δ-notation in per mil according to the following equation: $\delta = (R_{sample}/R_{standard} - 1) \times 1{,}000$, where R is the measured ratio of $^{13}C/^{12}C$ in the sample and Vienna PeeDee Belemnite standard (V-PDB). Analytical precision of isotope analyses was ≤0.10 ‰. TOC and TN were calculated according to the yield of $CO_2$ and $N_2$ after sample combustion in the elemental analyzer. Analytical precision was ±3 % (1 s) for carbon and ±2 % (1 s) for nitrogen. TOC of the decarbonized sample was back-calculated to the whole sample and results are presented in wt%. TOC and TN values were used to calculate atomic $C_{org}/N$ ratios.

The carbon isotopic composition of methane ($\delta^{13}C_{CH4}$) was determined on the same samples used for headspace chromatography. Duplicate measurements were processed with an IsoPrime® mass spectrometer connected to a trace gas preconcentrator. Results are given in standard δ-notation relative to V-PDB.

Pore water samples from core 5022-1A were obtained using soil moisture samplers (Rhizon® soil moisture samplers Eijkelkamp®) inserted into sediments through small holes drilled in the core liners. Fluids were extracted using syringes screwed to the Rhizons and maintained under low pressure. To avoid shifts in water chemistry, recovered samples were split for cation and anion analyses after sampling, and immediately flushed with helium gas. Samples for cation analyses were acidified with 100 µl $HNO_3$ (65 % suprapure). Transfer of pore water samples into sealed vials was performed under a $N_2$ atmosphere in a small chamber. Cations were determined by ICP-MS and anions were analyzed by ion-chromatography.

Minerals and matrices of authigenic concretions were observed using a binocular microscope (Nikon SMZ800 equipped with a Go-3 QImaging Digital USB Microscope Camera) and a scanning electron

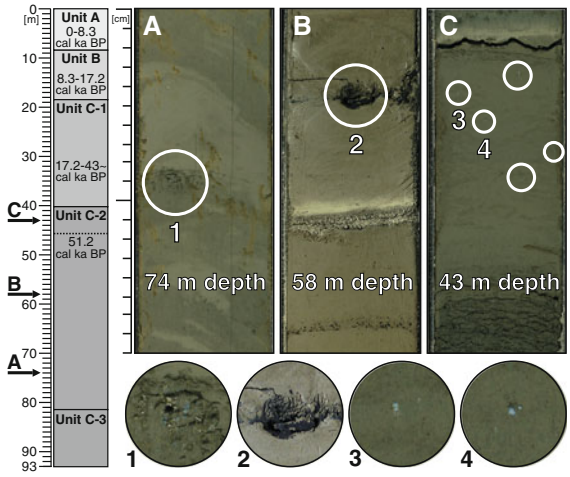


**Fig. 2** *Left* Synthetic log of Potrok Aike sedimentary record (after Kliem et al. 2012) with brief descriptions of the lithostratigraphic units. *Unit A* Pelagic laminated silts with presence of calcite *Unit B* Pelagic laminated silts, fine sand layers and gravity events. *Unit C-1* Pelagic laminated silts, fine sand layers and gravity events (thickness < 1 m). *Unit C-2* Pelagic laminated silts, fine sand layers and several gravity events (thickness up to 1 m). *Unit C-3* Sand and gravel layers, few pelagic laminated silts, fine sand layers and numerous gravity events (thickness > 1 m). Concretions, indicated by *arrows*, are all located within Unit C-2. *Right* Photographs of the sediment intervals containing authigenic vivanite. Basaltic tephra underlies each of these sequences. **A** Core 5022-1D at 74 m depth **B** core 5022-2A at 58 m depth, corresponding to a depth 53 m for site 1 **C** core 5022-1D at 43 m depth. Numbered circles (*1–4*) indicate the positions of the close-up pictures of the concretions and nuggets of vivianite

microscope (SEM) (Carl Zeiss EVO® 50). For SEM observation, dried samples were mounted on 12.7-mm-diameter aluminum stubs, using double-sided adhesive carbon discs. They were observed under variable pressure mode (10–400 Pa), enabling observation of non-conductive samples without metal coating. Such conditions prevent metal contamination and minimize the charge-up on the surface during observation. The Carl Zeiss EVO® 50 SEM is equipped with a Variable Pressure Secondary Electron detector (VPSE) for topographic images, a 4-Quadrant Backscattered electron Detector (QBSD) for backscattered electron (BSE) images, which allows viewing images in chemical contrast depending on the mean atomic number of the specimen, and an X-ray Energy Dispersive Spectroscopy (EDS) microanalysis system (model: INCAx-sight EDS detector, Oxford Instruments) for elemental analyses of surficial nanoparticles. The Lithium Drifted Silicon Si(Li) detector has a resolution of 133 eV and can identify elements from beryllium (Z = 4) to uranium (Z = 92) for concentrations >1,000 ppm. It must be operated close to liquid nitrogen temperatures. The accelerating voltage was 20 kV and working distances were 8.5 mm for BSE and 6.5 mm for secondary electron images. Additional imaging was also performed on coated samples with a Jeol JSM 7001F SEM. Prior to imaging, samples were mounted on aluminium stubs with double-sided conductive carbon tape, and an ultra-thin coating (~15 nm) of gold was deposited on the samples by low vacuum sputter coating with a Leica EM SCD 500 metallizer.

## Results

### Organic carbon in bulk sediment

The average TOC content in glacial sediments is very low with values often ≤0.3 % (Fig. 3A). Two horizons within the glacial record, however, display higher TOC values of 1.23 and 0.76 %, at 74 and at 37 m depth, respectively. TOC values along the Holocene record range between 0.3 and 2.0 %, with the highest TOC content around 10 m depth corresponding roughly to the late glacial/Holocene transition. Values then fluctuate between 0.3 and 1.5 % in the uppermost 10 m of sediment. TN (not shown) displays identical trends to those of TOC, but has lower average values, with a maximum of 0.25 % at 10 m sediment depth. From the core bottom up to 20 m depth, the atomic $C_{org}$/N ratio (Fig. 3A) displays very low values, with two exceptional peaks ≥10 within the mentioned glacial horizons, at 74 and 37 m depth. In the uppermost 20 m of sediment, the atomic $C_{org}$/N ratio increases from 4 to 10, and fluctuates between 6 and 12 along the Holocene record, reaching a maximum of 14 at 0.7 m depth. Carbon isotopes of bulk OM (Fig. 3A) show variations that are confined to the Holocene sediments. The glacial sediments display a uniform trend, with peaks of −25.1 and −24.0 ‰ around 70 m depth. From 10 to 5 m depth, $\delta^{13}C_{org}$ decreases from −24.1 to −27.8 ‰. From this depth to the top, the isotopic composition displays an increasing trend, reaching −23.0 ‰ in the uppermost sediments.

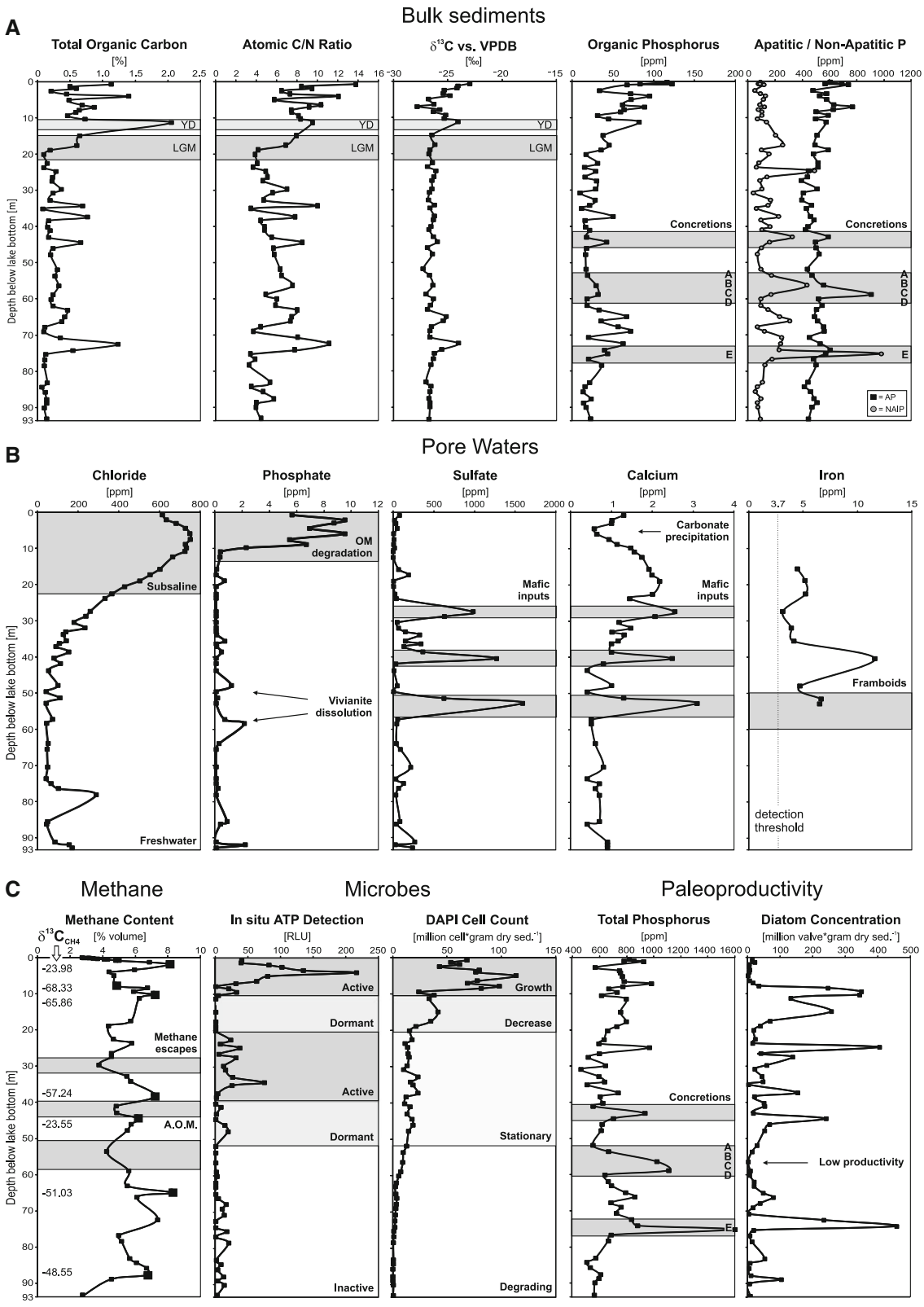
A
Bulk sediments
Total Organic Carbon
[%]
Atomic C/N Ratio
δ13C vs. VPDB
[‰]
Organic Phosphorus
[ppm]
Apatitic / Non-Apatitic P
[ppm]
Depth below lake bottom [m]
YD
LGM
Concretions
A
B
C
D
E
= AP
= NAIP
B
Pore Waters
Chloride
[ppm]
Phosphate
Sulfate
Calcium
Iron
Subsaline
Freshwater
OM degradation
Vivianite dissolution
Mafic inputs
Carbonate precipitation
Framboids
detection threshold
C
Methane
Microbes
Paleoproductivity
Methane Content
δ13CCH4
[% volume]
In situ ATP Detection
[RLU]
DAPI Cell Count
[million cell*gram dry sed.-1]
Total Phosphorus
Diatom Concentration
[million valve*gram dry sed.-1]
-23.98
-68.33
-65.86
-57.24
-23.55
-51.03
-48.55
Methane escapes
A.O.M.
Active
Dormant
Inactive
Growth
Decrease
Stationary
Degrading
Low productivity

◀ **Fig. 3** **A** Results for OM characterization on core 5022-1D. From *left* to *right* total Organic Carbon (TOC); atomic C/N ratio; $\delta^{13}C_{org}$ of the bulk sediment; Organic Phosphorus (OP); Apatite Phosphorus (AP) and Non-Apatite Inorganic Phosphorus (NAIP). *Grey* shadings highlight successively from *left* to *right*: The Late Glacial Maximum (LGM) and Younger Dryas (YD) chronozones, the sedimentary sequences presented in Fig. 2 and concretions labeled A–E from Fig. 4. **B** Results of pore water analyses from core 5022-1A. From *left* to *right* chloride; phosphate: *Arrows* indicate intervals of vivianite alteration; sulfate; calcium: The *arrow* indicates ikaite precipitation; iron: The disappearance of dissolved iron is linked to its precipitation as sulfides; *Grey* shadings highlight from *left* to *right*: Subsaline paleoconditions of the water column, the influence of organic matter degradation, mafic inputs related to the reworking of volcanites by gravity events, the interval where framboids were observed. **C** Results from core 5022-1D for methane, indexes related to microbial population and proxy indicators of paleoproductivity. From *left* to *right* methane content and results for methane carbon isotopes ($\delta^{13}C_{CH4}$) with AOM denoted by a maximum $\delta^{13}C_{CH4}$ value at 44.5 m sediment depth: Larger *squares* indicate samples on which $\delta^{13}C_{CH4}$ was measured; in situ ATP detection used as an index of microbial activity within sediments; DAPI cell counts indicating the density of microbes; TP of the bulk sediment; diatom concentration (modified after Recasens et al. 2012): The *arrow* indicates an interval of low algal productivity. *Grey* shadings highlight from *left* to *right*: Methane escapes associated with gravity events, different degrees of microbial activity, the evolution of microbial population density, the sediment sequences and concretions from Figs. 2 and 4

## Phosphorus speciation

Total phosphorus (TP) equals the sum of inorganic phosphorus (IP) and organic phosphorus (OP), and IP corresponds to the sum of apatite phosphorus (AP) and non-apatite inorganic phosphorus (NAIP). Figure 3A displays results for OP, AP and NAIP, whereas TP is shown in Fig. 3C. The OP content is high within the first glacial horizon at 74 m depth, whereas the highest values are in the uppermost 10 m of sediment. The OP content is greatest at 0.7 m depth, but decreases gradually from the surface down to 20 m. AP appears to be the dominant form of phosphorus, with an average content of 500–600 ppm throughout the sediment column. NAIP shows both increasing and decreasing trends, with sporadic peaks in the glacial record (75, 66, 56, 43 and 25 m depth). In the same broad interval, AP displays synchronous increases at about 75, 57 and 43 m depth. TP displays the highest values at these same depths, coinciding with vivianite concretions that were sampled subsequently. Within the uppermost 20 m, where no authigenic concretions were found, AP and NAIP contents differ significantly from one another and NAIP and OP contents are negatively correlated.

## Pore water analyses

Figure 3B displays pore water concentrations for chloride, phosphate, sulfate, calcium and iron. From 30 m to 5 m depth, chloride content increases gradually from 200 to 800 ppm, illustrating the shift of the water column from freshwater to subsaline conditions during the late glacial-Holocene transition. The data also show that pore waters reflect the original lake water composition and were not affected by diffusion of lake water into the sediments. The orthophosphate and OP profiles show similar trends, with high concentrations in the uppermost 10 m. In the glacial record, some low phosphate concentrations in pore waters are found at depths where concretions were observed, i.e. at 74, 58 and 43 m depth. Sulfate concentration in pore waters shows three sharp peaks, at 50, 49 and 25 m depth, which can be related to inputs of altered mafic tephra (Kliem et al. 2012). The same peaks can be identified for calcium in accordance with the mafic composition of such sediments. Otherwise, the calcium content decreases from 20 m to 5 m depth, concomitantly with the observed chloride increase. Dissolved iron concentrations in pore waters were often below the detection limit and very low concentrations were observed from 50 to 15 m depth, with a maximum value of 12 ppm at 38 m depth.

## Methane content and $\delta^{13}C_{CH4}$

Figure 3C shows total methane content in percent of the initial sample volume (3 ml = 3 $cm^3$). Large squares indicate samples in which $\delta^{13}C_{CH4}$ was measured and isotope values are listed next to the graph. Surface sediments show high methane content linked to the activity of methanogens. Below the surface, methane content decreases substantially from 2 to 8 m depth and rises again at 9 m depth. Below 20 m depth, methane content is quite variable.

The $\delta^{13}C_{CH4}$ value (Fig. 3C) at 2 m depth is −23.98 ‰ and decreases to −68.33 ‰ at 8 m depth. At 12 m depth, a peak in methane content coincides with a $\delta^{13}C_{CH4}$ value of −65.86 ‰. A much higher value (−23.55 ‰) is observed around 40 m depth, at the top of the interval containing framboids.

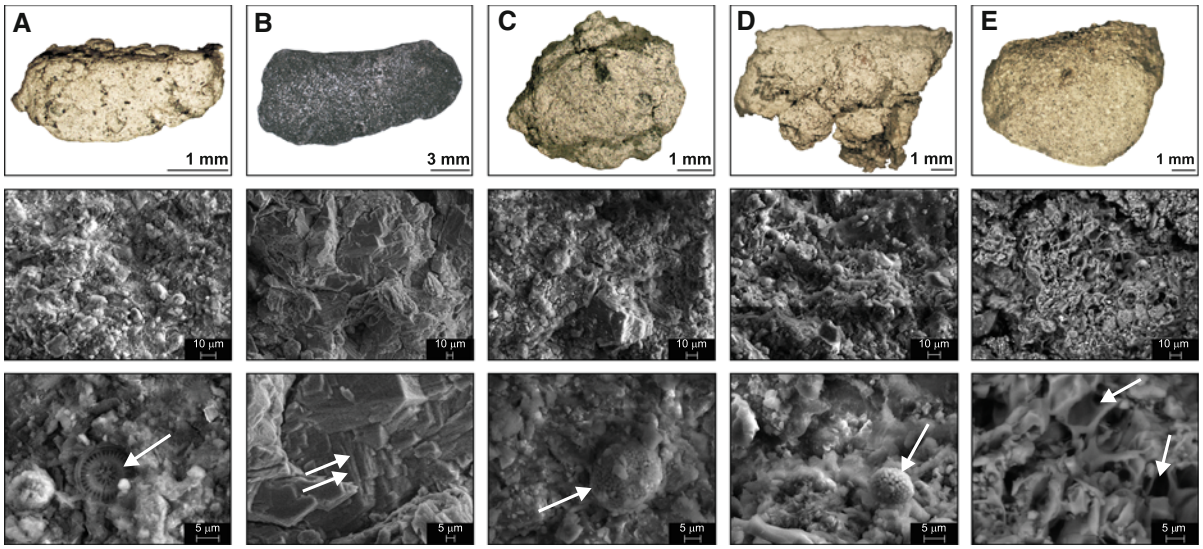


**Fig. 4** Images of concretions under increasing magnification using a binocular microscope (*first row*) reveal scattered *dark* minerals. Successive SEM close-up pictures (*second* and *third rows*) show different textures such as heterogenous, massive and porous. **A** Concretion showing an heterogenous texture with black-opaque-minerals, diatoms (*white arrow*), and clays (core 5022-2A; sites 1/2 depth: 53/57 m). **B** Block of massive vivianite, pictured after oxidation and fading of its *blue* color (core 5022-2A; site 1/2 depth: 53/57 m) showing a single composition with perfect cleavage (*white arrows*). **C** Concretion of fine texture showing black minerals, altered clays (microbial?) and framboids (*white arrow*) (core 5022-2B, site 1/2 depth: 57/66 m). **D** Concretion of fine texture with black minerals, altered clays (microbial?) and framboids (white arrow) (core 5022-2B; site 1/2 depth: 59/67 m). **E** Concretion apparently composed of volcanic vesicular material (*white arrows*) from tephra (core 5022-2C; site 1/2 depth: 74/79 m)

## Microbial population activity and density

In situ ATP measurements (Fig. 3C) show a sharp increase from the surface down to 4 m depth, followed by a strong decrease down to 8 m depth. Small increases are then seen at 9, 34 and 49 m depth, along with some slightly higher TOC and OP values for the glacial record (Fig. 3A). DAPI cell counts (Fig. 3C) decrease from the surface to 3 m and then increase to a maximum value at 5 m depth. The microbial population density fluctuates below that depth, and decreases dramatically at 9 m. Then it stabilizes at a low density, decreasing gradually down to 60 m, where it almost disappears. A small peak, however, is evident at 34 m.

## Microscopic observations

### *Concretions*

Concretions shown in Fig. 4A–E were recovered from clayey layers of sediment sequences, composed of mafic sands at the base, overlain by clays topped with a very thin horizon (Fig. 2) at 56.96, 66.23, 67.14 and 78.58 m depth in the site 2 composite core (Gebhardt et al. 2011), corresponding approximately to 46, 53, 57, 58 and 74 m depth in the site 1 composite core (Recasens et al. 2012). Concretion B is a blue and blocky vivianite mass (Nuttin et al. 2012) that quickly faded away after core opening (Fig. 2B2). Observation under increasing magnification revealed a massive texture of a single composition. The perfect cleavage of vivianite is even visible under the highest magnification (Fig. 4B, right). Observation of concretions A, C, D and E under reflected light shows they are <1 cm in diameter (Fig. 4 top). SEM images exhibit textural heterogeneities, such as variable sizes of incorporated grains dominantly in fine matrixes, as well as the presence or absence of cementation. The highest SEM magnification provided the most interesting information, as specific components appeared entangled within the concretions. Indeed, concretion A is rich in diatom frustules. Concretions C and D show framboids within foliated clays, also associated with what is most probably exopolymeral substances

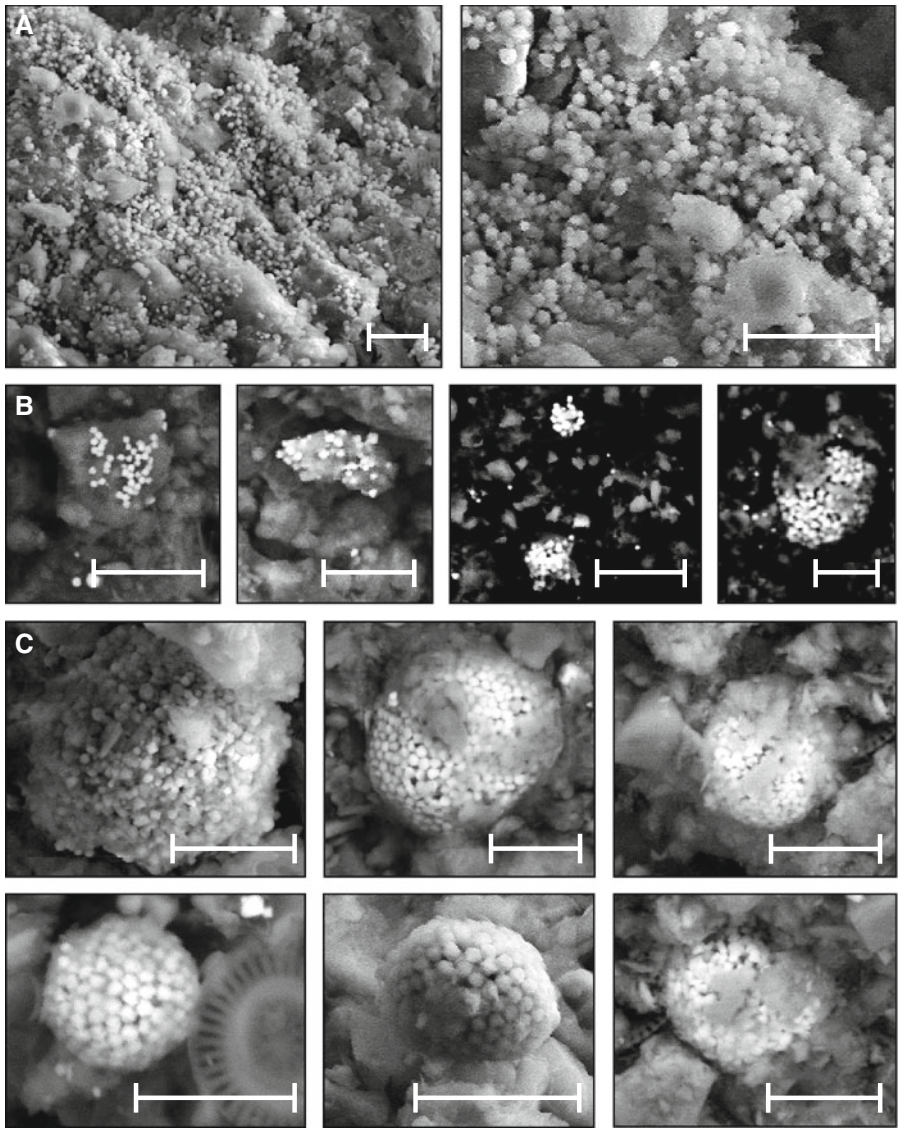


**Fig. 5** SEM microphotographs of framboid precursors and framboids. **A** Disseminated single cubic crystals of iron sulfides (scales = 10 μm). **B** BSE images of partially aggregated iron sulfide crystals, possibly showing the stepwise process of framboid aggregation (scales = 10 μm), **C** fully formed framboids (scales = 10 μm)

(EPS). Concretion E is mainly composed of porous volcanic material.

*Framboids and precursors*

Framboids and their precursors were identified in concretions A, C and D. Numerous microcrystals of iron sulfide are displayed in Fig. 5A, illustrating an initial stage of nucleation (Wilkin et al. 1996). The different framboids presented in Fig. 5C display a rather homogenous size distribution, with diameters ranging between 10 and 15 μm.

*EDS elemental analyses*

EDS analyses were performed on phosphates (Fig. $6A_{1–4}$), framboids (Fig. $6B_{1–4}$), matrices and specific foliated clays (Fig. $6C_{1–2}$) and some accessory mineral (ESM 2). Iron oxides such as hematite ($Fe_2O_3$), magnetite ($Fe_3O_4$), or ilmenite ($FeTiO_3$) were

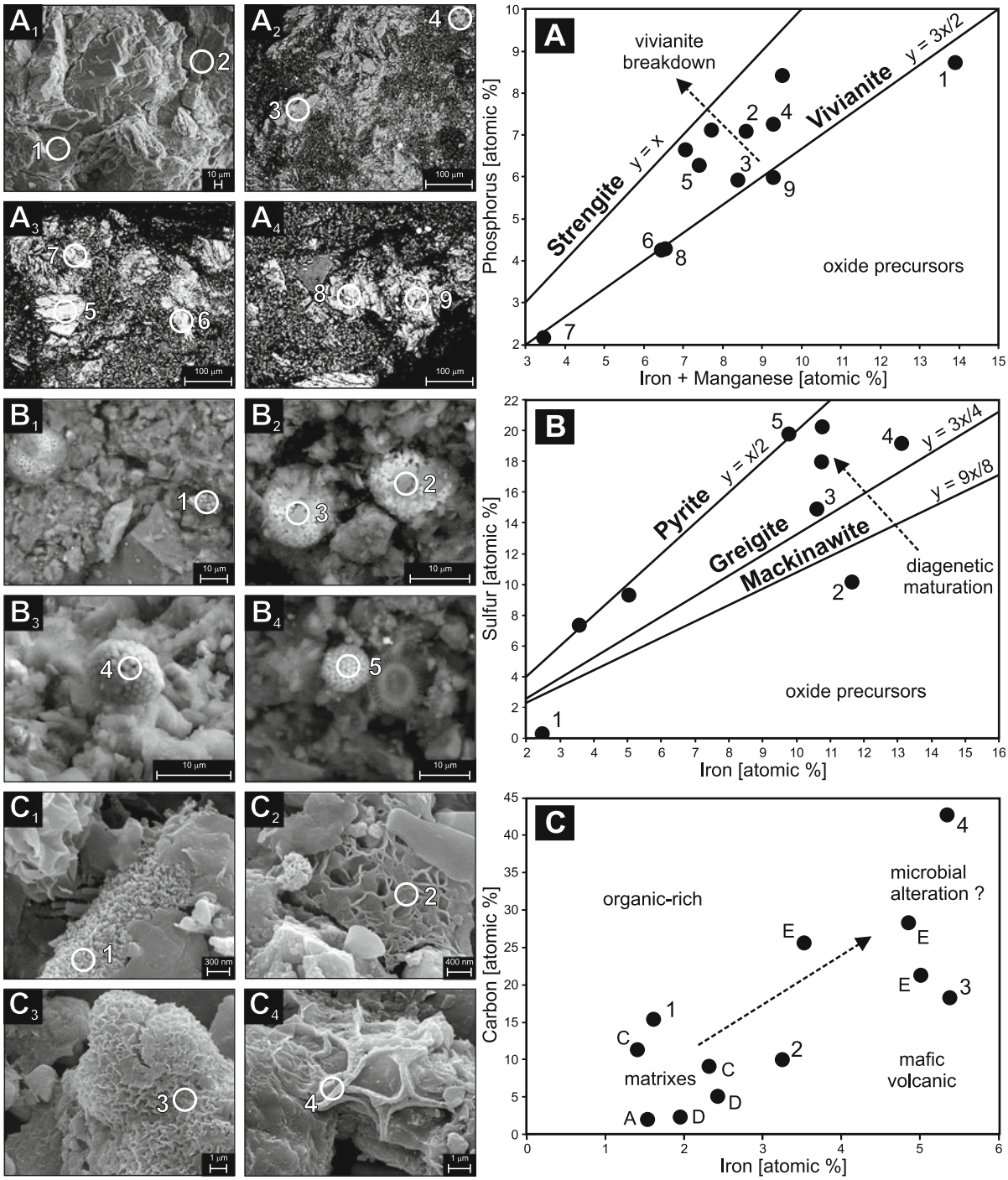


**Fig. 6** SEM images showing the position of points analyzed by EDS and their results are plotted on the *right*. Pictures $C_{1–4}$ were taken on coated samples. **A** phosphates, **B** framboids, **C** matrices and foliated minerals interpreted as altered smectites. $C_4$ represents remnants of microbial EPS. $C_{1–2}$ and $C_{3–4}$ depths are 0.75 m and 60 m, respectively

not investigated because they are very common in the catchment, and thus mostly from detrital origin. BSE images were used to distinguish phosphates within matrices. Vivianite ($Fe_3(PO_4)_2{\cdot}8H_2O$) was the dominant identified mineral, although anapaite ($Ca_2Fe(PO_4)_2{\cdot}4H_2O$), another authigenic phosphate, was also

identified once. Analyses that did not match the stoichiometric ratio for vivianite perfectly were considered alteration byproducts of this mineral that most often turn to strengite ($Fe^{2+}PO_4{\cdot}2H_2O$). EDS measurements on framboids (Fig. 6B) reveal a range of compositions corresponding mainly to greigite and pyrite. The lines on the plots shown in Fig. 6A, B (right side) correspond to stoichiometric compositions of specific phosphorus- and sulfur-containing minerals, respectively. Carbon and iron content of matrices were also plotted (Fig. 6C, right side) to assess the possible sorption of organic elements onto oxides. Additional analyses were carried out on coated samples that revealed specific clays habitus (Fig. $6C_{1–3}$) and EPS remnants (Fig. $6C_4$). These results show a positive correlation between carbon and iron contents, leading to an inference for coupled iron and OM reduction in the presence of microbes.

## Discussion

### Conditions for authigenic mineral formation

#### *Vivianite*

In Laguna Potrok Aike the influence of mafic volcanics on sediment geochemistry (Kliem et al. 2012) seems to have played a major role in the formation of the studied concretions. Reworking of mafic scoria and ashes from the catchment (Fig. 1) could have provided large amounts of the necessary phosphate, iron and sulfur (Park et al. 2005), whereas associated oxides (Manning et al. 1999) and smectites (Stamatakis and Koukouzas 2001) would have been ideal phosphorus sinks. Smectites are alteration products of soils and volcanic ashes and are known to occur within the Potrok Aike sediment record, where they represent up to 50 % of the clay fraction (Nuttin et al. 2012). Overall, different forms of phosphorus throughout the core reflect variations in the sedimentation regime. Sedimentary sequences (Fig. 2) of basaltic sands, overlain by thin clayey horizons, suggest sporadic inputs of AP followed by sedimentation of adsorbed NAIP (Fig. 3A). AP is insoluble and generally of detrital origin (Zhou et al. 2001). Authigenic apatite is known to form only in marine environments (Compton et al. 2007) and thus is not part of this lacustrine record. AP variations reflect changes in allochthonous input into the Potrok Aike closed basin corresponding with gravity events during the glacial interval (Kliem et al. 2012). NAIP is a bioavailable form of phosphorus that turns into an authigenic form when adsorbed onto metal oxides within the sediment, thereby restricting its solubility in sediments to reducing conditions (Anderson et al. 2001). The coupled AP and NAIP behavior can be explained by external input of phosphorus with AP, its insoluble form, which settles directly to the sediment. At the same time, NAIP is dissolved in the water column and precipitates within fine particles when adsorbed onto metal oxides (Hupfer et al. 1998). Vivianite precursors such as HFO, green rust and hydroxyphosphates (Nriagu and Dell 1974; Fredrickson et al. 1998), are known to form by the adsorption of phosphorus onto iron oxides (Fagel et al. 2005). These accumulations are transformed into vivianite during methanic diagenesis (Berner 1981). In lacustrine systems, this process has often been reported in surficial sediments (Emerson 1976; Berner 1981; Sapota et al. 2006), with frequent occurrences in anoxic, low-sulfide sedimentary environments (Manning et al. 1999) and cold, dry climate zones (Sapota et al. 2006). The low TOC content in Laguna Potrok Aike glacial sediments (Fig. 3A) is an additional factor that could have favored P fixation in the sediment (Wang et al. 2007) and limited bacterial P release from sediments (Gächter et al. 1988). Additionally, the frequent gravity events during the glacial period (ESM 1) reflect higher sedimentation rates that disrupted the microbial degradation chain that would otherwise favor quick OM mineralization and thereby prevented P diffusion to the water column.

Holocene sediments of Laguna Potrok Aike illustrate the opposite situation, with a pelagic to hemipelagic sedimentation (Kliem et al. 2012). Their high pore-water phosphate concentrations (Fig. 3B) were probably caused by OM degradation and associated high microbial activity (Fig. 3C) along with low sulfate concentrations (Fig. 3B). Subsequent mineralization of OP degraded by microbes may trigger the formation of authigenic forms of phosphate (Gächter et al. 1988), as indicated by the gradual increase of NAIP in bulk sediment down to 20 m depth. Such inverse correlation between OP and NAIP was only observed in relatively young sediments as the preservation potential of OP forms in older sediments is very low and does not allow discrimination between sorption processes and mineralization. Remobilization

of authigenic forms of NAIP can occur under reducing conditions with solubilization back to the water column (Wang et al. 2007) or to interstitial waters (Zhou et al. 2001; Compton et al. 2007). Moreover, small concentrations of $H_2S$ from sulfate reduction destabilize vivianite, possibly remobilizing its iron to sulfides and dissolving small amounts of phosphate from the concretions in deep glacial sediments (Fig. 3B). Thus, this ability of vivianite to shift from a P sink to P source within the sediment highlights the fact that caution must be used if vivianite is to be utilized as a paleoindicator of prevailing environmental conditions during its formation.

*Framboids*

The iron sulfide framboids (Fig. 5C) display rather small and homogenous sizes without overgrowth (Schieber 2002). Such features are probably formed within sediment porewaters under anoxic conditions (Wilkin et al. 1996; Suits and Wilkin 1998; Böttcher and Lepland 2000), rather than in the water column (Park et al. 2005). The different composition of the framboids (Fig. 6B) may result from the variety of reactive iron available (Fig. 3B) and variable redox conditions (Berner 1981; Wilkin et al. 1996). Indeed, slightly sulfided iron oxides were detected in partial aggregates (Fig. 5B), mackinawite ($Fe_9S_8$) and greigite ($Fe_3S_4$), sometimes as fully formed framboids (Fig. 6B). Greigite as a ferrimagnetic precursor to framboidal pyrite, has been documented in other lacustrine settings (Ariztegui and Dobson 1996) and implies gradual diagenetic maturation. The sulfide iron oxides have been interpreted as precursors of pyrite ($FeS_2$), which is the dominant framboidal mineral (Wilkin and Barnes 1997) formed from interstitial anoxic waters (Suits and Wilkin 1998; Böttcher and Lepland 2000) and probably mediated by microbial activity (Astafieva et al. 2005). The presence of dissolved iron above the framboid-containing interval (Fig. 3B) argues for iron reduction coupled with sulfate reduction, to account for precipitation of iron ($Fe^{2+}$) sulfides below 40 m depth. Development of framboids is linked to microcrystal aggregation by magnetic attraction (Wilkin and Barnes 1997). This plausible path of framboid formation is shown in Fig. 5B. Because availability of reactive iron is the dominant control on pyrite formation (Berner 1981), production of $H_2S$ via sulfate reduction is sufficient to transform sulfide precursors such as mackinawite and greigite into pyrite (Holmer and Storkholm 2001). Concomitant measurement of in situ ATP and DAPI cell count at ~50 and ~40 m depth (Fig. 3C) is evidence for the sustainability of such microbial processes.

*Carbonate and other minerals*

There are abundant carbonate crystals in the two uppermost lithostratigraphic units of the Laguna Potrok Aike record (Kliem et al.2012; Nuttin et al. 2012), whereas they are completely absent in late glacial sediments, aside from some reworked gastropod shells. Oehlerich et al. (2012) found that carbonate precipitates in modern Laguna Potrok Aike as mm-sized ikaite ($CaCO_3{\cdot}6H_2O$), which rapidly disintegrates into μm-sized calcite crystals. These fine calcite crystals are morphologically identical to the calcite in the rest of the sediment record, which supports the idea that these carbonates were originally precipitated as ikaite in the water column and transformed to calcite soon thereafter. Although ikaite is normally metastable, it precipitates when calcite and aragonite nucleation is inhibited by low temperatures and high phosphate concentrations (Oehlerich et al. 2012). Carbonate precipitation today is favored by the salinity increase during lake-level lowstands of the presently closed-basin waterbody (Ohlendorf et al. 2012). Chloride and calcium profiles (Fig. 3B) reflect a salinity increase within the upper 20 m, with an increase in chloride and a decrease in calcium, the latter a consequence of carbonate precipitation.

Some accessory minerals were also encountered within the studied concretions (ESM 2). Ilmenite, magnetite and plagioclase ($NaAlSi_3O_8$-$CaAl_2Si_2O_8$) were also identified, reflecting detrital input from the surrounding igneous rocks.

## Early diagenesis and timing of authigenic mineral formation

*Microbial mediation*

In situ ATP production and high microbial population densities (Fig. 3C) provide evidence for substantial

microbial reduction processes within the topmost 10 m of sediment (Konhauser 2007). Simultaneous presence of framboids and vivianite is explained by a series of anaerobic processes related to stratified microbial communities (Nealson and Stahl 1997). Iron reduction is the first step, followed by sulfate reduction, whereby the produced $H_2S$ reacts with dissolved iron and precipitates as iron sulfides. Methanogenesis generally starts only after sulfate depletion (Hoehler et al. 2001) and reduces vivianite precursors. High sulfate concentrations in some sediment horizons of the glacial record (Fig. 3B), however, would greatly limit methane production (Schubert et al. 2011), as sulfate reducers are known to outcompete methanogens (Schink 2002). The decrease in methane content from 2 to 8 m depth (Fig. 3C) could be explained by redeposition events, as suggested by geophysical data in the lake (Anselmetti et al. 2009), or preferential bacterial use of the substrate (Hoehler et al. 2001; Schink 2002). The high methane content at ~10 m depth (Fig. 3C) is associated with a sudden shift of $\delta^{13}C_{CH4}$ towards lower values (~−68 ‰), indicating methane production based on $^{13}C$-depleted compounds, as would be the case with advanced $CO_2$ reduction (Whiticar 1999). High variability of methane below 20 m depth is interpreted as the result of low TOC content within late glacial sediments, along with frequent gravity events during this time interval (Fig. 3C). These gravity event deposits, composed of mafic volcanics, supplied iron and sulfate to the basin, causing microbial iron and sulfate reduction in such mafic horizons. Simultaneously, associated high sediment loads disrupted methanogenesis in underlying organic clays and triggered methane escapes to the overlying sediments (Fig. 3C and ESM 1). At the same time, NAIP was adsorbed on volcanic clays and iron oxides in the water column and precipitated as fine sediments. A succession of discrete mafic sand and organic clay horizons could lead in turn to competing processes, such as sulfate reduction and methanogenesis. Indeed, the shift of $\delta^{13}C_{CH4}$ toward higher values at ~40 m depth (Fig. 3C) demonstrates that methane was used as a source of carbon, with residual methane enriched in $^{13}C$ (Valentine 2002; Schubert et al. 2011). A common byproduct of sulfate reduction and anaerobic oxidation of methane (AOM) is concurrent precipitation of pyrite (Schink 2002). It is still unclear, however, whether these diagenetic products were formed at shallow depths or after a longer burial time.

*Depth of formation*

Nuttin et al. (2012) demonstrated that the vivianite concretions in Potrok Aike experienced diffusion of elements to and from the surrounding sediments through time. U-Th dating gave ages much younger than the model deposition age (Kliem et al.2012) and were thus attributed to late diagenetic precipitation under open system conditions.

In the uppermost 10 m of sediment, the NAIP content (Fig. 3A) remains low, whereas a large fraction of the phosphorus is found as OP and phosphate in pore waters (Fig. 3A, B). Because microbes are abundant and active throughout the Holocene record (Fig. 3C), P remineralization rates during early diagenetic stages render uncertain the formation depth of vivianite. Furthermore, microbial activity in Potrok Aike sediments is sustained as deep as 40 m (Fig. 3C) and authigenesis can thus be considered a slowly evolving process. At the same time, high sedimentation rates related to gravity events favored the adsorption and mineralization of phosphorus by disrupting the methanogenic degradation chain, while inputs of sulfur into the system further promoted sulfate reduction over methanogenesis. In situ ATP detections at 48 and 34 m depth (Fig. 3C) imply that there are still substantial ongoing microbial processes at these depths, with possible sites of reduced activity at 70 and 80 m depth, associated with relatively high TOC and OP contents for the glacial record. AOM and microbially mediated pyrite formation are good examples of deep survival strategies of sulfate reducers (Schink 2002). Moreover, microbial iron reduction is known to provoke alteration of different clay minerals, especially in the presence of sulfate (Li et al. 2004), leading to significant structural changes in clay lattices (Stucki and Kostka, 2006). Besides, SRB have the ability to reduce iron-containing minerals to support their growth (Li et al. 2004; Zhang et al., 2012). Smectites, which are the most abundant clay group in Potrok Aike sediments, may originate from the weathering of mafic rocks, but from authigenic processes as well. Nuttin et al. (2012) reported a gradual decrease in their 2θ angle peak with depth, which is commonly observed with microbial alteration (Dong et al. 2009). During microbial reduction of Fe(III) from smectites, the mineral structure has to be stabilized by the addition of interlayer cations, the habitus becoming foliated

during the process (Dong et al. 2009), and as they lose their sorption capacity, altered smectites tend to release adsorbed nutrients (Kostka et al. 1999; Stucki and Kostka 2006). Figure 6$C_{1-3}$ show OM interbedded with clays with different degrees of foliation. Their respective depths, along with EPS remnants (Fig. 6$C_4$), indicate clay-microbe interactions, with microbial metabolism possibly increasing clay alteration over time (Zhang et al. 2012). Anoxic releases of Fe and P (Fig. 3B) from metal oxides and sediments could also result from the activity of the microbial consortium (Gächter et al. 1988; Li et al. 2004), making the elements available to the bacteria, with methane as a complementary source of carbon. Further consumption of released phosphate in the presence of reduced iron leads to vivianite precipitation (Dong et al. 2009). Although culture studies on bacterial iron reduction have shown that vivianite is a stable end product (Glasauer et al. 2003), some levels of phosphate content (Fig. 3B) seem to be associated with vivianite dissolution (Wilson et al. 2010). Vivianite could be an alternative source of phosphorus that sustains microbial communities (Smith and Prairie 2004). AOM, smectite alteration and the associated release of adsorbed organics are critical to maintain microbial activity in deep environments, thus continuing to support diagenetic processes. The microbial signal does, however, become difficult to track below 40 m sediment depth in our record, where it begins to fade.

*Paleo-indicator or biosignature*

Comparison of TOC, TN and NAIP (Fig. 3A) suggests that iron and phosphorus in the concretions were derived from both volcanic sources and OM mineralization. Evidence for these two different sources is found in the material incorporated in the concretions. Pumice found in concretions C, D and E (Fig. 4) illustrates the role of mafic inputs, whereas the framboids attest to microbial reduction processes. In parallel, diatom concentration peaks (Fig. 3C) that coincide with TP and NAIP argue for gravity events and associated loads of P and Fe as a trigger of blooms in the water column (Recasens et al. 2012). Moreover, methane escapes, along with high calcium, sulfate and AP values (Fig. 3C, B and A), show sudden contributions of substantial mafic material reworked into the basin (ESM 1, sample D40). Concretions B–D (Fig. 4), however, possess low diatom counts (Fig. 3C), demonstrating the buffering effect on primary productivity of P adsorption and sequestration in vivianite (Nriagu 1972). The high numbers of diatom frustules in sediments (Fig. 3C) and concretion a (Fig. 4A) provide evidence for the recovery of primary production. The concretions reflect both nutrient enrichment of the lake basin and P sequestration from the water column as a result of sporadic inputs of catchment material, and thus offer potential insights into paleoproductivity during the glacial period (Fagel et al. 2005). The same applies to smectites as they could be derived from weathered volcanic ashes and soils associated with greater precipitation or aeolian transport (Nuttin et al. 2012). Because vivanite can be altered easily, it remains an unreliable paleoindicator.

The use of the studied concretions as biosignatures depends upon the respective diagenetic role of chemical adsorption and microbial remineralization in their formation (Hupfer et al. 1998). Although large concretions (Fig. 2B) result from precipitation via oxide precursors reduced during methanic diagenesis (Berner 1981; Fagel et al. 2005), nuggets of vivianite scattered in the sediments (Fig. 2A–C) reflect precipitation from pore waters after OM degradation and P remineralization by microorganisms (Gächter et al. 1988; Manning et al. 1999). Culture experiments have shown that vivianite formation only occurs in the presence of sufficient $Fe^{2+}$ and IP, along with microbial respiration (Glasauer et al. 2003). Other indirect signs of microbially mediated vivianite formation include clay alteration, methane production, and possibly framboids. Aside from the fact that methanogens are capable of dissolving clay minerals and further triggering vivianite aggregates, they are easily inhibited by DIRB and outcompeted by SRB under adequate Fe(II) and $SO_4$ interstitial concentrations (Zhang et al. 2012). Methanogenesis limitation could be inferred from moderate $\delta^{13}C_{CH4}$ values (−48.55 to 57.24 ‰) (Fig. 3C), which might result from relatively low isotopic fractionation during methane formation.

Whether framboids can be considered biosignatures is still a matter of debate because natural crystals are hardly distinguishable from their synthetic abiogenic counterparts. Previous studies in sedimentary environments found fossilized microbial features associated with framboids (Schieber 2002; MacLean

et al. 2008). On the other hand, the conditions required to nucleate such pyrites abiotically (Ohfuji and Rickard 2005) drastically diminish the possibility of such a pathway in lacustrine sediments. Although microbial features were not unequivocally detected on SEM microphotographs, some signs indicate the microbial origin of these framboids (Fig. 5C). They include low ATP (Fig. 3C), $\delta^{13}C_{CH4}$ values (Fig. 3C) linked to AOM and sulfate reduction (Schink 2002), gradual maturation (Fig. 6B) and related concentration shifts in pore waters (Fig. 3B), P release from vivianite destabilized by production of $H_2S$ (Fig. 3B), along with possible smectite alteration (Fig. $6C_{1-2}$) caused by structural iron reduction (Kostka et al. 1999; Li et al. 2004).

## Conclusions

We conclude that, 50–45 ka ago, deposition of reworked volcanic material into Potrok Aike maar, related to gravity events, played a dominant role in forming authigenic concretions in the sediments. Large amounts of OM were adsorbed onto oxides and smectites, partially controlling the lake trophic status. The low OM content of glacial sediments favored P retention, in authigenic form, during burial. Early diagenetic processes linked to stratified microbial communities may explain the concomitant formation of vivianite and iron sulfides. Methanogenesis appeared initially as the dominant process during early diagenesis, but was often disrupted by sporadic gravity events as a consequence of lake level declines during the glacial. Mafic volcanics reworked from the catchment to the lake basin acted as the main supply of iron, sulfur and phosphorus, thus influencing primary productivity and generating additional microbial metabolism. In fine organic sediments, methane production reduced IP complexed to volcanic clays and iron oxides to form vivianite concretions, whereas iron and sulfate reduction started replacing methanogenesis in mafic horizons. Microbial iron and sulfate reduction were sustained throughout diagenesis and led to the formation of framboids. Mackinawite and greigite evolved towards pyrite, implying diagenetic maturation through the sediment record. Additional evidence of prolonged microbial influence during diagenesis includes in situ ATP detection below 30 m depth, AOM process as indicated by $\delta^{13}C_{CH4}$, and possible microbial alteration of smectites. In the meantime, methane and phosphorus consumption by microbes likely caused the nucleation of vivianite from sediment interstitial waters.

In summary, results from this study emphasize the successive influence of volcanic materials on microbial metabolism, leading to the formation of mineral concretions. Furthermore, sustained microbial activity observed within sediments shows that processes such as mineral authigenesis and diagenesis can be under their prolonged influence. Although authigenic minerals *per se* do not constitute unequivocal biosignatures, the multiple lines of evidence used to investigate concretions in Laguna Potrok Aike indicate diagenetic processes, mediated by microbial activity, during their formation. These features can be used to reconstruct authigenic and/or diagenetic processes in similar lake basins at different geographic and temporal scales.

**Acknowledgments** Funding for this study was provided by ICDP; Swiss National Science Foundation (Grant 200020-119931/2 to D. Ariztegui) and University of Geneva, Switzerland; University of Bremen and Deutsche Forschungsgemeinschaft, Germany; Natural Sciences and Engineering Research Council of Canada; University of Buenos Aires and Secretaria de Ciencia y Tecnologia of Cordoba, Argentina; and the Vetenskapsrädet of Sweden, and Eawag. P. Arpagaus and S. Becker are kindly acknowledged for the phosphorus speciation analyses and the ICP-MS pore water results, respectively. W. Klöti is acknowledged for processing with methane headspace analyses and G. Nobbe for doing the carbon isotopes on methane. We also thank A. Lisé-Pronovost for providing the picture in Fig. 2B and for first describing the presence of vivianite in the Laguna Potrok Aike sediments. We kindly acknowledge the comments and suggestions of two reviewers on an earlier version of the manuscript, and M. Brenner for his help in editing the present paper.

## References

Anderson LD, Delaney ML, Faul KL (2001) Carbon to phosphorus ratios in sediments: implications for nutrient cycling. Glob Biogeochem Cycles 15:65–79

Anselmetti FS, Ariztegui D, De Batist M, Gebhardt AC, Haberzettl T, Niessen F, Ohlendorf C, Zolitschka B (2009) Environmental history of southern Patagonia unraveled by the seismic stratigraphy of Laguna Potrok Aike. Sedimentology 56:873–892

Ariztegui D, Dobson J (1996) Magnetic investigations of framboidal greigite formation: a record of anthropogenic environmental changes in eutrophic Lake St Moritz, Switzerland. Holocene 6:235–241

Astafieva MM, Rozanov AY, Hoover R (2005) Framboids: their structure and origin. Paleontol Zh 39:457–464

Berner RA (1981) Authigenic mineral formation resulting from organic matter decomposition in modern sediments. Fortschr Miner 59:117–135

Beveridge TJ, Meloche JD, Fyfe WS, Murray RGE (1983) Diagenesis of metals chemically complexed to bacteria: laboratory formation of metal phosphates, sulfides, and organic condensates in artificial sediments. Appl Environ Microbiol 45:1094–1108

Böttcher ME, Lepland A (2000) Biogeochemistry of sulfur in a sediment core from the west-central Baltic Sea: evidence from stable isotopes and pyrite textures. J Mar Syst 25:299–312

Compton J, Mallinson D, Glenn CR, Filippelli G, Föllmi K, Shields G, Zanin Y (2007) Variations in the global phosphorus cycle. SEPM Special Publ 66(66):21–33

Dong H, Jaisi DP, Kim J, Zhang G (2009) Microbe-clay mineral interactions. Am Miner 94:1505–1519

Emerson S (1976) Early diagenesis in anaerobic lake sediments: chemical equilibria in interstitial waters. Geochim Cosmochim Acta 40:925–934

Fagel N, Alleman LY, Granina L, Hatert F, Thamo-Bozso E, Cloots R, André L (2005) Vivianite formation and distribution in Lake Baikal sediments. Glob Planet Change 46:315–336

Fredrickson JK, Zachara JM, Kennedy DW, Dong H, Onstott TC, Hinman NW, Li S-M (1998) Biogenic iron mineralization accompanying the dissimilatory reduction of hydrous ferric oxide by a groundwater bacterium. Geochim Cosmochim Acta 62:3239–3257

Gächter R, Meyer JS, Mares A (1988) Contribution of bacteria to release and fixation of phosphorus in lake sediments. Limnol Oceanogr 33:1542–1558

Gebhardt AC, De Batist M, Niessen F, Anselmetti FS, Ariztegui D, Haberzettl T, Kopsch C, Ohlendorf C, Zolitschka B (2011) Deciphering lake and maar geometries from seismic refraction and reflection surveys in Laguna Potrok Aike (southern Patagonia, Argentina). J Volcanol Geotherm Res 201:357–363

Glasauer S, Weidler PG, Langley S, Beveridge TJ (2003) Controls of Fe reduction and mineral formation by a subsurface bacterium. Geochim Cosmochim Acta 67:1277–1288

Haberzettl T, Corbella H, Fey M, Janssen S, Lücke A, Mayr C, Ohlendorf C, Schäbitz F, Schleser GH, Wille M, Wulf S, Zolitschka B (2007) Lateglacial and Holocene wet-dry cycles in southern Patagonia: chronology and geochemistry of a lacustrine record from Laguna Potrok Aike, Argentina. Holocene 17:297–310

Hoehler TM, Alperin MJ, Albert DB, Martens CS (2001) Apparent minimum free energy requirements for methanogenic Archaea and sulfate-reducing bacteria in an anoxic marine sediment. FEMS Microbiol Ecol 38:33–41

Holmer M, Storkholm P (2001) Sulphate reduction and sulphur cycling in lake sediments: a review. Freshw Biol 46:431–451

Hupfer M, Fischer P, Friese K (1998) Phosphorus retention mechanisms in the sediment of an eutrophic mining lake. Water Air Soil Pollut 108:341–352

Kliem P, Enters D, Hahn A, Ohlendorf C, Lisé-Pronovost A, St-Onge G, Wastegård S, Zolitschka B and the PASADO science team (2012) Lithology, radiocarbon chronology and sedimentological interpretation of the lacustrine record from Laguna Potrok Aike, southern Patagonia. Q Sci Rev. PASADO special issue, available online August 2012. doi:10.1016/j.quascirev.2012.07.019

Konhauser K (2007) Introduction to geomicrobiology. Blackwell Science Ltd, Oxford

Kostka JE, Wu J, Nealson KH, Stucki JW (1999) The impact of structural Fe(III) reduction by bacteria on the surface chemistry of smectite clay minerals. Geochim Cosmochim Acta 63:3705–3713

Li Y-L, Vali H, Sears SK, Yang J, Deng B, Zhang CL (2004) Iron reduction and alteration of nontronite NAu-2 by sulfate-reducing bacterium. Geochim Cosmochim Acta 68:3251–3260

Lovley DR (1997) Microbial Fe(III) reduction in subsurface environments. FEMS Microbiol Rev 20:305–313

MacLean LCW, Tyliszczak T, Gilbert PUPA, Zhou D, Pray TJ, Onstott TC, Southam G (2008) A high-resolution chemical and structural study of framboidal pyrite formed within a low-temperature bacterial biofilm. Geobiology 6:471–480

Manning PG, Prepas EE, Serediak MS (1999) Pyrite and vivianite in the bottom sediments of eutrophic Baptiste Lake, Alberta, Canada. Can Miner 37:593–601

Mayr C, Lücke A, Maidana NI, Wille M, Haberzettl T, Corbella H, Ohlendorf C, Schäbitz F, Fey M, Janssen S, Zolitschka B (2009) Isotopic fingerprints on lacustrine organic matter from Laguna Potrok Aike (southern Patagonia, Argentina) reflect environmental changes during the last 16,000 years. J Paleolimnol 42:81–102

Nauhaus K, Boetius A, Krüger M, Widdel F (2002) In vitro demonstration of anaerobic oxidation of methane coupled to sulphate reduction in sediment from a marine gas hydrate area. Environ Microbiol 4(5):296–305

Nealson KH, Stahl DA (1997) Microorganisms and biogeochemical cycles: what can we learn from layered microbial communities? Rev Miner 35:5–34

Nriagu JO (1972) Stability of vivianite and ion-pair formation in the system Fe3(PO4)2-H3PO4-H2O. Geochim Cosmochim Acta 26:459–470

Nriagu JO, Dell CI (1974) Diagenetic formation of iron phosphates in recent lake sediments. Am Miner 59:934–946

Nuttin L, Francus P, Preda M, Ghaleb B, Hillaire-Marcel C (2012) Authigenic, detrital and diagenetic minerals in the Laguna Potrok Aike sedimentary sequence. Q Sci Rev. PASADO special issue, available online December 2012. doi:10.1016/j.quascirev.2012.09.027

Oehlerich M, Mayr C, Griesshaber E, Lücke A, Oeckler OM, Ohlendorf C, Schmahl WW, Zolitschka B (2012) Ikaite precipitation in a lacustrine environment—implications for paleoclimatic studies using carbonates from Laguna Potrok Aike (Patagonia, Argentina). Q Sci Rev. PASADO special issue, available online June 2012. doi:10.1016/j.quascirev.2012.05.024

Ohfuji H, Rickard D (2005) Experimental syntheses of framboids—a review. Earth-Sci Rev 71:147–170

Ohlendorf C, Fey M, Gebhardt C, Haberzettl T, Lücke A, Mayr C, Schäbitz F, Wille M, Zolitschka B (2012) Mechanisms of lake-level change at Laguna Potrok Aike (Argentina)—insights from hydrological balance calculations. Q Sci Rev. PASADO special issue, available online November 2012. doi:10.1016/j.quascirev.2012.10.040

Park MH, Kim JH, Ryu BJ, Yu KM (2005) Tephrostratigraphy and paleo-environmental implications of Late Quaternary

sediments and interstitial water in the western Ulleung Basin, East/Japan Sea. Geo-Mar Lett 25:54–62

Postma D (1981) Formation of siderite and vivianite and the pore-water composition of a recent bog sediment in Denmark. Chem Geol 31:225–244

Recasens C, Ariztegui D, Gebhardt AC, Gogorza C, Haberzettl T, Hahn A, Kliem P, Lisé-Pronovost A, Lücke A, Maidana N, Mayr C, Ohlendorf C, Schäbitz F, St-Onge G, Wille M, Zolitschka B, The PASADO Science Team (2012) New insights into paleoenvironmental changes in Laguna Potrok Aike, Southern Patagonia, since the Late Pleistocene: the PASADO multiproxy record. Holocene 22:1323–1335

Ross P-S, Delpit S, Haller MJ, Németh K, Corbella H (2011) Influence of the substrate on maar-diatreme volcanoes—an example of a mixed setting from the Pali Aike volcanic field, Argentina. J Volcanol Geotherm Res 201:253–271

Sapota T, Aldahan A, Al-Aasm IS (2006) Sedimentary facies and climate control of formation of vivianite and siderite microconcretions in sediments of Lake Baikal, Siberia. J Paleolimnol 36:245–257

Schieber J (2002) Sedimentary pyrite: a window into the microbial past. Geology 30:531–534

Schink B (2002) Synergistic interactions in the microbial world. Antonie Van Leeuwenhoek 81:257–261

Schubert CJ, Vazquez F, Lösekann-Behrens T, Knittel K, Tonolla M, Boetius A (2011) Evidence for anaerobic oxidation of methane in sediments of a freshwater system (Lago di Cadagno). FEMS Microbiol Ecol 76:26–38

Smith EM, Prairie YT (2004) Bacterial metabolism and growth efficiency in lakes: the importance of phosphorus availability. Limnol Oceanogr 49:137–147

Stamatakis MG, Koukouzas NK (2001) The occurrence of phosphate minerals in lacustrine clayey diatomite deposits, Thessaly, Central Greece. Sediment Geol 139:33–47

Stucki JW, Kostka JE (2006) Microbial reduction of iron in smectite. C. R. Geosci 338:468–475

Suits NS, Wilkin RT (1998) Pyrite formation in the water column and sediments of a meromictic lake. Geology 26:1099–1102

Valentine DL (2002) Biogeochemistry and microbial ecology of methane oxidation in anoxic environments: a review. Antonie Van Leeuwenhoek 81:271–282

Vuillemin A, Ariztegui A and the PASADO Scientific Team (2012) Geomicrobiological investigations of lake sediments over the last 1500 years. Q Sci Rev. PASADO special issue, available online May 2012, doi:10.1016/j.quascirev.2012.04.011

Wang S, Jin X, Zhao H, Zhou X, Wu F (2007) Effect of organic matter on the sorption of dissolved organic and inorganic phosphorus in lake sediments. Colloid Surface A 297: 154–162

Whiticar MJ (1999) Carbon and hydrogen isotope systematics of bacterial formation and oxidation of methane. Chem Geol 161:291–314

Wilkin RT, Arthur MA (2001) Variations in pyrite texture, sulfur isotope composition, and iron systematics in the Black Sea: evidence for Late Pleistocene to Holocene excursions of the $O_2$-$H_2S$ redox transition. Geochim Cosmochim Acta 65:1399–1416

Wilkin RT, Barnes HL (1997) Formation processes of framboidal pyrite. Geochim Cosmochim Acta 61:323–339

Wilkin RT, Barnes HL, Brantley SL (1996) The size distribution of framboidal pyrite in modern sediments: an indicator of redox conditions. Geochim Cosmochim Acta 60:3897–3912

Wilson TA, Amirbahman A, Norton SA, Voytek MA (2010) A record of phosphorus dynamics in oligotrophic lake sediment. J Paleolimnol 44:279–294

Zachara JM, Fredrickson JK, Li SM, Kennedy DW, Smith SC, Gassman PL (1998) Bacterial reduction of crystalline $Fe^{3+}$ oxides in single phase suspensions and subsurface materials. Am Miner 83:1426–1443

Zelibor JL, Senftle FE, Reinhardt JL (1988) A proposed mechanism for the formation of spherical vivianite crystal aggregates in sediments. Sediment Geol 59:125–142

Zhang J, Dong H, Liu D, Fischer TB, Wang S, Huang L (2012) Microbial reduction of Fe(III) in illite-smectite minerals by methanogen *Methanosarcina mazei*. Chem Geol 292–293: 35–44

Zhou Q, Gibson C, Zhu Y (2001) Evaluation of phosphorus bioavailability in sediments of three contrasting lakes in China and the UK. Chemosphere 42:221–225

Zolitschka B, Schäbitz F, Lücke A, Corbella H, Ercolano B, Fey M, Haberzettl T, Janssen S, Maidana N, Mayr C, Ohlendorf C, Oliva G, Paez MM, Schleser GH, Soto J, Tiberi P, Wille M (2006) Crater lakes of the Pali Aike Volcanic Field as key sites for paleoclimatic and paleoecological reconstructions in southern Patagonia, Argentina. J S Am Earth Sci 21:294–309